

# Observation of sub-Poissonian correlation in spin-orbit coupled polariton vortex pairs at room temperature

Xiaokun Zhai,<sup>1</sup> Ying Gao,<sup>1</sup> Xuekai Ma,<sup>2</sup> Chunzi Xing,<sup>1</sup> Xiao Wang,<sup>3</sup>  
Anlian Pan,<sup>3</sup> Marc Assmann,<sup>4</sup> Stefan Schumacher,<sup>2,5,6</sup> and Tingge Gao<sup>1</sup>

<sup>1</sup>*Department of Physics, School of Science, Tianjin University, Tianjin 300072, China*

<sup>2</sup>*Department of Physics and Center for Optoelectronics and Photonics Paderborn (CeOPP),  
Universität Paderborn, Warburger Strasse 100, 33098 Paderborn, Germany*

<sup>3</sup>*College of Materials Science and Engineering, Hunan University, Changsha 410082, China*

<sup>4</sup>*Department of Physics, Otto-Hahn-Str. 4a, TU Dortmund University, 44227 Dortmund, Germany*

<sup>5</sup>*Institute for Photonic Quantum Systems (PhoQS),  
Paderborn University, 33098 Paderborn, Germany*

<sup>6</sup>*Wyant College of Optical Sciences, University of Arizona, Tucson, AZ 85721, USA*

Coupling of orbital and spin degrees of freedom gives rise to intriguing physical phenomena in bosonic condensates, such as formation of stripe phases and domains with vortex arrays. However, the robust locking of spin and orbital degrees of freedom of the nonlinear topological objects such as vortex pairs with sub-Poissonian fluctuation in bosonic condensates remains challenging. In the present work, we realize a non-equilibrium room-temperature condensate in a liquid crystal (LC) planar photonic microcavity with the perovskite CsPbBr<sub>3</sub> as optically active material. We use the interplay of TE-TM mode splitting and Rashba-Dresselhaus spin-orbit coupling (RDSOC) to realize electrically tunable polariton vortex pairs with locked spin and orbital angular momentum. Remarkably, the counts difference between opposite wavevector states shows sub-Poissonian fluctuation, indicating the existence of the correlation between the two vortices. Our results are robust against sample imperfections and pave the way to investigate coupling and locking of correlated vortex orbital and spin degrees of freedom in a quantum fluid of light at room temperature, offering potential for generation of complex squeezed states of light for quantum optical information processing with optoelectronic chips.

Coupling of spin and orbital degrees of freedom of particles determines the intrinsic properties of many materials. Enabling the control of spin degrees of freedom in solids [1, 2], spin-orbit coupling (SOC) plays a critical role in spintronics and topological insulators [3–7]. In the regime of equal Rashba [8] and Dresselhaus [9] spin-orbit coupling infinite spin lifetime [10], spin helices and spin precession were demonstrated [3, 4] in a two dimensional electron gas. In bosonic cold atom condensates, synthetic spin-orbit coupling is explored, which can be controlled by careful engineering of the spin states of atoms with laser beams. There, for example the transition from a spin-mixed phase to a spin-separated phase [11] and the measurement of a stripe phase [12] in a one dimensional Rashba and Dresselhaus coupled cold atom gas have been realized. By tuning the Raman coupling strength and introducing spatially dependent detuning which creates an effective magnetic field in the RDSOC regime [13–15], vortices or vortex lattices can be formed [16–18]. In these systems, complicated arrangement of multiple lasers is needed to realize the underlying Hamiltonians with effective SOC. In addition, sub-Poissonian correlation between the vortices with locked quantized orbital angular momentum (OAM) and spin angular momentum (SAM) is very difficult to realize, which can find important application in quantum information processing using squeezed macroscopic states [19–23].

In this work we demonstrate the sub-Poissonian correlation between exciton polariton vortex pairs with locked

spin and orbital degrees of freedom that form as robust topological objects in the nonlinear regime in a photonic planar microresonator at room temperature. In such optical systems correlated vortices formed with well defined and locked spin and orbital degrees of freedom play an increasingly important role for communication technologies and qubit manipulation schemes [24–26]. As depicted in Figure 1(a), our realization constitutes a liquid-crystal (LC) planar photonic microcavity with the perovskite CsPbBr<sub>3</sub> as optically active material. The LC allows to tune the spatial anisotropy and related effective refractive indices with an externally applied electric field, such that an effective RDSOC [27] is realized with the separation of the two opposite spin components in the momentum space and real space [28]. More importantly, these spin splittings mean that a photon with the wavevector  $k_y$  is accompanied by another photon with the wavevector  $-k_y$ , which indicates the correlation between these states.

The particles underlying our system are hybrid quasi-particles, so-called exciton polaritons, that are created due to the strong coupling of excitons in the perovskite material and cavity photons [29, 30]. These have attracted significant attention for the manipulation of vortex states [31–35] for instance and enabled by the large exciton binding energy and oscillator strength in the perovskite material show condensation up to room temperature [36–40]. A splitting between longitudinal and transversal optical modes (or TE-TM splitting) is intrinsic

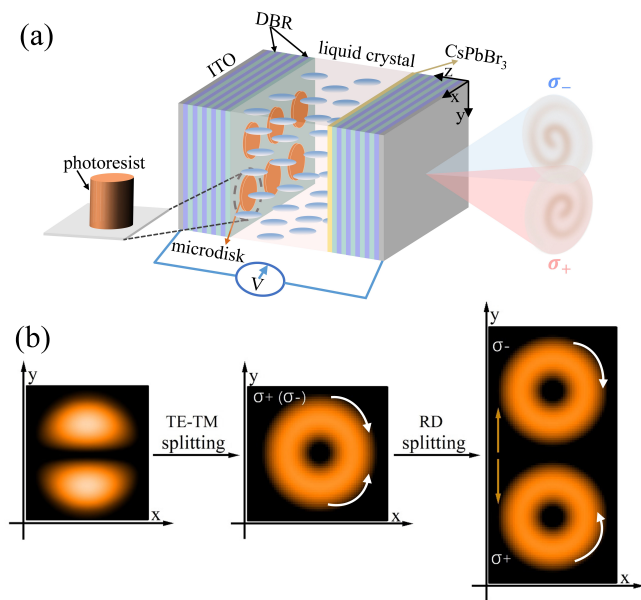


**FIG. 1. Schematic of the liquid crystal microcavity and formation of spin-orbit coupled vortex pairs.** (a) The DBR microcavity is filled with liquid crystal and contains a microdisk potential array on one side and perovskite  $\text{CsPbBr}_3$  microplates on the other side. (b) Sketch of the idealized (nonlinear) modes for different types of spin-orbit coupling: the TE-TM splitting splits a polariton dipole mode into two spin-orbit-locked vortices, which are stabilized and spatially separated by the Rashba-Dresselhaus coupling with sub-Poissonian correlation.

sis to such planar microcavities and acts as an effective magnetic field, in the linear regime giving rise to the optical spin Hall effect [41–43]. In the nonlinear regime, the TE-TM splitting influences the nonlinear modes formed: considering a setting with near rotational symmetry and spatially confined topological modes with finite orbital angular momenta, a dipole mode (left graph in Figure 1(b)) is split into two vortices with topological charges locked with the vectorial polarization degree of freedom, or in other words, locked with the SAM [44]. The underlying linear modes can be obtained by numerically solving the Schrödinger equation  $[H + V]\Psi = E\Psi$ , with confinement potential  $V$  in the circular shape as illustrated in the middle graph of Figure 1(b) and discussed in more detail in the SM. However, these kinds of well defined spin-orbit locked modes that also form a natural basis for the interpretation of the nonlinear condensate modes have not yet been observed in experiments at room temperature. With only weak TE-TM splitting, a very high-quality microcavity would be required as otherwise detrimental factors such as sample disorder or nonlinear interactions between polaritons tend to destroy the locking between SAM and OAM.

In the present work, we show that the combined influence of significant TE-TM splitting and RDSOC spa-

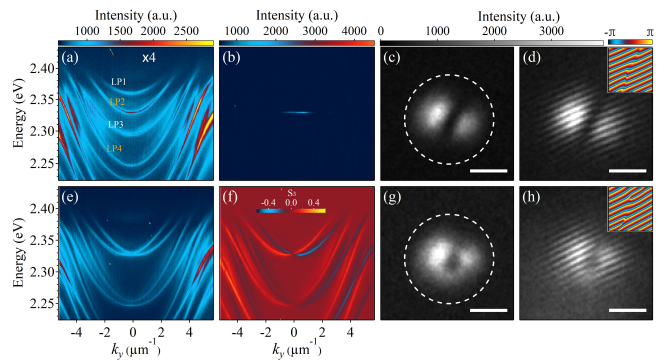


**FIG. 2. Polariton condensation in the liquid crystal microcavity at different voltages.** (a, b) Dispersion below and above threshold at 5 V. (c, d) Real space image and interferogram of the polariton condensate above threshold at 5 V. (e) Dispersion below threshold at 5.6 V. (f) Spin polarized dispersion at 5.6 V. (g, h) Real space image and interferogram of the polariton condensate above threshold at 5.6 V. The dashed lines in (c) and (g) show the microdisk location. The insets in (d, h) show the extracted phase distribution. The scale bars:  $2 \mu\text{m}$ .

tially separates the two spin polarized components in a polariton condensate above threshold [36], such that each spin component carries a distinct OAM. This results in the formation of spin-orbit locked vortex pairs, in which vortices in opposite SAM components are stabilized and can directly be observed by measuring the left- and right-circularly polarized condensate emission at room temperature (cf. the right panel in Figure 1(b)). By virtue of the prominent vortex separation in the momentum space, we find that the population number difference with opposite wavevector  $\pm k_y$  shows sub-Poissonian fluctuation, which confirms that the polariton vortex pairs are correlated in the RDSOC regime. These findings are robust against disorder within the microcavity. Our results demonstrate a new mechanism to electrically create well defined correlated states with locked spin and orbital degrees of freedom in a quantum fluid of light. Compared with other optically tunable spin-orbit coupled photonic vortex lasers [25, 26, 45] or polariton vortices confined in micropillar structures, which so far are limited to cryogenic temperature [46], our work lays the foundation to manipulate electrically tunable sub-Poissonian correlated state with spin-orbit coupled angular momentum based on quantum fluids of light at room temperature.

In the experiments we introduce photoresist microdisk structures with the diameter of  $4 \mu\text{m}$  (the distance between the microdisk is around  $15 \mu\text{m}$  to avoid interaction) and the height of  $120 \text{ nm}$  onto the bottom Distributed Bragg Reflector (DBR) using lithography technique in the LC microcavity, where the effective cavity length of the microdisk is larger and the cavity mode energy is smaller compared with other area. The details

of the microcavity is shown in Figure 1(a). In this case, the microdisks act as potential traps and polaritons are confined in these structures, occupying the specific discrete energy levels [47, 48], for example, a dipole mode (see Figure 1(b) and the SM). The size of the inserted CsPbBr<sub>3</sub> microplates is around 40  $\mu\text{m}$  which can cover at least one microdisk potential. We use a linearly polarized femtosecond laser (frequency: 1 kHz, wavelength: 400 nm, pulse width: 50 fs) to excite the microcavity with the size of around 50  $\mu\text{m}$  and collect the photoluminescence from the sample using a home-made angle-resolved spectroscopy setup.

The electric field onto the ITO surface of the microcavity is realized by using a function generator. We measure the dispersion of the LC microcavity below threshold when the voltage is 5 V, which is plotted in Figure 2(a). Multiple polariton branches are observed when the pumping density is far below the threshold due to the large thickness of the cavity. That is, several cavity modes exist within the microcavity and strongly couple with the excitons (detailed fitting parameters using the coupled oscillator model are shown in the SM). The dispersions with much larger curvatures originate from the signal out of the perovskite microplates. The strong coupling is confirmed at the large-wavevector region where one can clearly observe that the dispersions become flat when approaching the exciton resonance. Under this voltage, the LP1 and LP3 are horizontally linearly polarized whereas the LP2 and LP4 are vertically linearly polarized.

With further increasing the pumping density to around 18  $\mu\text{J}/\text{cm}^2$ , the emitted PL intensity of the polaritons increases superlinearly, whereas the linewidth drops suddenly and the polariton energy shows noticeable continuous blueshift (details can be found in the SM). These results clearly show the occurrence of the polariton condensation at the lower branch LP2 (Figure 2(b)). In the near field, the condensed polaritons exhibit as a dipole mode above the threshold with the orientation determined by the anisotropy of the potential, see Figure 2(c). The condensate with a dipole distribution originates from the complicated energy relaxation and kinetics of discrete energy levels within the microdisk potential [46]. We build a Michelson interferometer where one arm is expanded by around 15 times and acts as the reference beam. Clear interference fringes are observed above the threshold (Figure 2(d)), the extracted phase from the Fast Fourier transformation of the fringes shown in the upper right corner indicates the development of the macroscopic coherence across the condensate and the phase jump of  $\pi$  across the two lobes.

TE-TM splitting is prominent in anisotropic perovskite-based microcavities [49, 50], which can decompose the above dipole mode into two vortices with the topological charge of  $\pm 1$ , locked with the SAM. However, the disorder within perovskite microplates

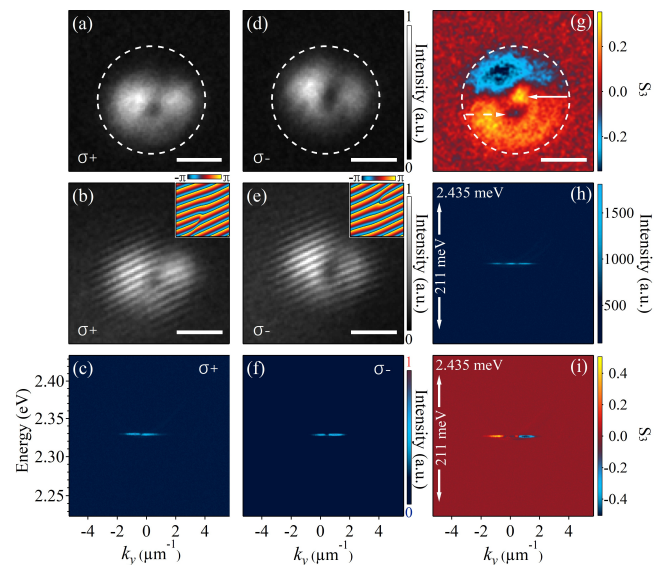


**FIG. 3. Spin-orbit locked vortex pair in the Rashba-Dresselhaus regime at 5.6 V.** (a) Real space image of the  $\sigma+$  component at 5.6 V. (b) Interferogram of the polariton condensate in (a). (c) Dispersion of the polariton condensate in (a). (d) Real space image of the  $\sigma-$  component at 5.6 V. (e) Interferogram of the polariton condensate in (d). (f) Dispersion of the polariton condensate in (d). (g) Spin polarized real space images corresponding to (a) and (b). The arrows indicate the location of the two vortex cores. (h, i) The total and spin polarized dispersion of the polariton condensate. The dashed lines in (a) and (d) show the microdisk location. The insets in (b) and (e) are the extracted condensate phase distributions. The scale bars: 2  $\mu\text{m}$ .

or photoresist microdisk can affect the stability or formation of the vortices. In addition, the nonlinear interaction between the polaritons can also destroy the locking between the SAM and OAM, thus preventing the observation of the spin-orbit locked vortices. As analyzed above, the stability of the vortices can be enhanced due to the RDSOC, which can be realized by increasing the voltage simply in our experiments. Under a higher voltage, the electric field rotates the LC molecular director which alters the anisotropic refractive index distribution within the microcavity plane. In this case, the horizontally linearly polarized modes LP1 and LP3 are tuned towards high energy, while the vertically linearly polarized modes LP2 and LP4 remain fixed. Under the voltage of 5.6 V, the polariton branch LP3 is blueshifted to be resonant with LP2. These two polariton branches have the opposite linear polarizations and parity, thus the RD spin split bands form (Figure 2(e)), which is confirmed in the spin polarized dispersion in Figure 2(f) where the dispersion shift of the two spin components along the  $k_y$  direction can be clearly seen.

In the near field, when the voltage increases from 5 V to 5.6 V, the dipole mode deforms under the same pumping density as can be seen in Figure 2(g) where the

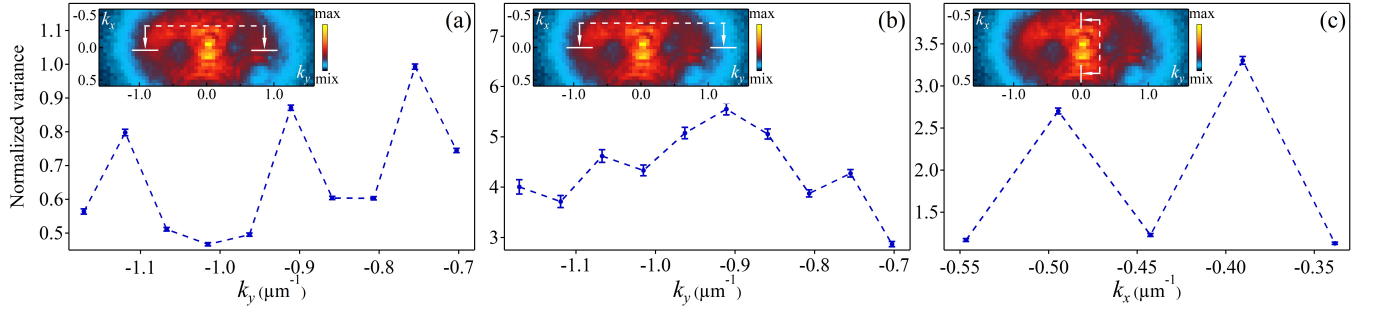


FIG. 4. **Sub-Poissonian fluctuation of counts difference variance in the momentum space.** (a) Counts difference variance between the states with opposite  $k_y$  ( $-1.17 \mu\text{m}^{-1} \sim -0.7 \mu\text{m}^{-1}$  vs  $1.17 \mu\text{m}^{-1} \sim 0.7 \mu\text{m}^{-1}$ ,  $k_x=0$ ), showing the sub-Poissonian fluctuation. (b) Counts difference variance between the states with non-opposite  $k_y$  ( $-1.17 \mu\text{m}^{-1} \sim -0.7 \mu\text{m}^{-1}$  vs  $1.43 \mu\text{m}^{-1} \sim 0.96 \mu\text{m}^{-1}$ ,  $k_x=0$ ). (c) Counts difference variance between the states with opposite  $k_x$  ( $-0.55 \mu\text{m}^{-1} \sim -0.34 \mu\text{m}^{-1}$  vs  $0.55 \mu\text{m}^{-1} \sim 0.34 \mu\text{m}^{-1}$ ,  $k_y=0$ ). The inserted graphs are the momentum space images and the lines in each of the images show the calculated zones.

polariton condensate carries a ring shape, indicating the formation of vortices. The interferogram of the polariton condensate in Figure 2(h) shows the emergence of two forks orientated in opposite directions. This confirms the existence of two vortices with the topological charge of  $\pm 1$  close to the core region of the ring-shaped condensate, which can be unambiguously proven by the extracted phase plotted at the upper right corner, calculated by using the same method as in Figure 2(d).

To check whether the two vortices are locked with the definite SAM as we analyzed above, we measure the right- and left-hand circularly polarized PL emitted from the microcavity, which correspond to different spins states of the polariton condensate. In Figure 3(a), an intensity minimum in the center of the polariton condensate is clearly visible in the  $\sigma+$  component, indicating the existence of a vortex. We note that the intensity distribution is not very symmetric around the intensity minimum, this is due to the inhomogeneity within the microcavity. From the interferogram by superimposing the real space image of the polariton condensate onto the reference arm, a fork is clearly observed, confirming the appearance of a vortex with the topological charge of 1, as plotted in Figure 3(b). The phase singularity can also be seen in the calculated phase distribution inserted at the upper right corner. From the dispersion taken under this voltage (Figure 3(c)), two peaks are observed to be located at the wavevector of  $0.12 \mu\text{m}^{-1}$  and  $-0.88 \mu\text{m}^{-1}$ , which is not symmetric along the normal incidence due to the RDSOC induced shift along  $k_y$  direction. This kind of particular distribution of the dispersion confirms the appearance of the vortex with asymmetric distribution in the momentum space for the  $\sigma+$  component.

On the other hand, in the  $\sigma-$  component, both the intensity minimum in the real space imaging (Figure 3(d)) and the fork in the interferogram graph (Figure 3(e)) demonstrate the formation of the vortex with the topological charge of -1. The location of the polariton con-

densate is shifted upwards, thanks to the RDSOC induced shift in the real space. In this spin component, the polariton condensate distribution in the momentum space is also shifted to the opposite direction compared to Figure 3(c), with the peak locations at  $0.98 \mu\text{m}^{-1}$  and  $-0.07 \mu\text{m}^{-1}$  (Figure 3(f)). The mode distribution of the dispersion clearly confirms the existence of the swapped topological charge of the vortex in the  $\sigma-$  component.

The appearance of the spin-orbit locked polariton vortex pair under 5.6 V originates from the synthetic magnetic field due to the RDSOC and the prominent TE-TM splitting. The nonzero TE-TM splitting can be confirmed by measuring the two linearly polarized dispersion along  $k_x$  direction when  $k_y = 0$  where the RDSOC disappears, shown in the SM. In our experiments, the TE-TM splitting decomposes the dipole mode into two spin-orbit locked vortices, whereas the RDSOC separates these vortices, thus the inter-species nonlinear interaction can be reduced. In this case, the two vortices are stabilized by the SOC in the microcavity and can be observed easily. The spin polarized real space imaging of the polariton condensate at 5.6 V plotted in Figure 3(g) demonstrates the separation of the two vortices along  $y$  direction with two cores clearly visible indicated by the arrows. The total (Figure 3(h)) and spin polarized dispersion (Figure 3(i)) along  $k_y$  direction also confirm the separation of the  $\sigma+$  and  $\sigma-$  components in the RDSOC regime, which are consistent with the polariton vortex distribution shown in Figure 3(g).

To demonstrate the sub-Poissonian correlation between the vortices, we calculate the counts difference in the momentum space within 101 continuous measurements (the exposure time for each experiment is 2 s, one momentum space image under 5.6 V is shown in the inserted graph in Figure 4(a, b, c)). Considering the width of the momentum spread within the polariton condensate, we calculate the wavevector-resolved counts difference variance in the range of  $-1.17 \mu\text{m}^{-1} \sim -0.7$

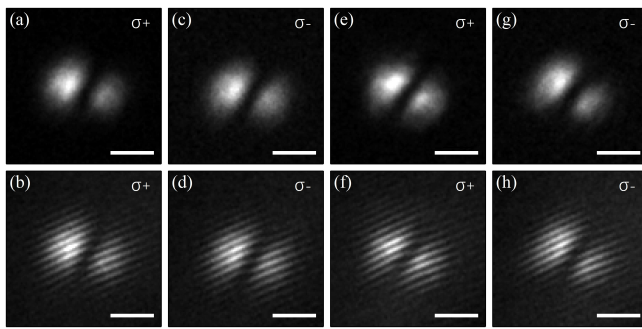


FIG. 5. **Nonlinear modes and polarization dependence of polariton condensates outside the Rashba-Dresselhaus regime.** (a, b) Real space image and interferogram of the  $\sigma+$  polarized component of the polariton condensate at 5 V. (c, d) Real space image and interferogram of the  $\sigma-$  polarized component of the polariton condensate at 5 V. (e-h) Same as (a-d) but for an external voltage of 6 V. The scale bars are  $2 \mu\text{m}$ .

$\mu\text{m}^{-1}$  by using the formula [23]:  $V_{ij} = (\langle (N_i - N_j)^2 \rangle - \langle (N_i - N_j) \rangle^2) / (\langle (N_i + N_j) \rangle)$ , where  $N_i$  and  $N_j$  represent the counts with the wavevector of  $k_y^i$  and  $k_y^j$  (the details of calculation can be found in the SM). Note that the wavevector range of  $-0.31 \mu\text{m}^{-1} \sim 0.31 \mu\text{m}^{-1}$  is not considered due to the overlap between the two vortices. The counts difference variance shows clear sub-Poissonian fluctuation with  $V_{ij} < 1$  when their wavevectors are opposite (Figure 4(a),  $k_x=0$ ), whereas  $V_{ij}$  is larger than 1 between the states with non-opposite  $k_y$  (Figure 4(b),  $k_x=0$ ) and with opposite  $k_x$  (Figure 4(c) where  $k_y=0$ ). This confirms that the two polariton vortices are correlated. We note that the sub-Poissonian fluctuation can be observed even the intensity of the single wavevector state has large fluctuation, shown in the SM.

If the RDSOC spin splitting disappears, for example, at 5 V where the polariton mode LP3 is far below LP2, the spin-orbit locking vanishes. As a result, the two spin components of the polariton condensate share the same spatial mode distribution in the real space without definite vorticity and spin polarization (Figure 5(a-d)). When the voltage applied to the microcavity is increased to 6 V (such that LP3 is tuned above LP2; see the SM), the polariton condensate also assumes a dipole shape. The  $\sigma+$  and  $\sigma-$  spin-polarized components of the polariton condensate again show the same spatial mode without vorticity due to the absence of the SOC (Figure 5(e-h)).

To summarize, we observe sub-Poissonian correlation between spin-orbit locked polariton vortex pairs in a LC microcavity with  $\text{CsPbBr}_3$  perovskite microplates as optically active material. The spin-orbit locked polariton vortices originate from the TE-TM splitting. They become observable due to the stabilization and real space separation of the condensate resulting from the synthetic

field from the RDSOC, and show sub-Poissonian fluctuation in the momentum space. Our results illustrate an important electrical method for the manipulation of sub-Poissonian correlation in spin-orbit locked topological states based on a quantum fluid of light at room temperature, and pave the way to investigate Cauchy-Schwarz inequality or squeezing using hybrid macroscopic light-matter particles at room temperature. These observations are of interest also for other areas such as cold atom gases and 2D electron gases in which the targeted design of spin-orbit locked states is often not accessible or much more complex to achieve.

TG acknowledges support from the National Natural Science Foundation of China (grant No. 12174285). The Paderborn group acknowledges support by the Deutsche Forschungsgemeinschaft (German Research Foundation) through the transregional collaborative research center TRR142/3-2022 (231447078, project A04) and by Paderborn Center for Parallel Computing, PC<sup>2</sup>.

- 
- [1] A. Manchon, H. C. Koo, J. Nitta, S. M. Frolov, R. A. Duine, New perspectives for Rashba spin-orbit coupling. *Nature Materials* **14**, 871-882 (2015).
  - [2] R. Winkler, S. J. Papadakis, E. P. De Poortere, M. Shayegan, *Advances in Solid State Physics: Spin-Orbit Coupling in Two-Dimensional Electron and Hole Systems*, vol 41 (Springer, Berlin, Heidelberg, 2003).
  - [3] Y. K. Kato, R. C. Myers, A. C. Gossard, D. D. Awschalom, Observation of the spin Hall effect in semiconductors. *Science* **306**, 1910-1913 (2004).
  - [4] M. König, S. Wiedmann, C. Brüne, A. Roth, H. Buhmann, L. W. Molenkamp, X. L. Qi, S. C. Zhang, Quantum spin Hall insulator state in HgTe quantum wells. *Science* **318**, 766-770 (2007).
  - [5] C. L. Kane, E. J. Mele,  $Z_2$  topological order and the quantum spin Hall effect. *Physical Review Letters* **95**, 146802 (2005).
  - [6] B. A. Bernevig, T. L. Hughes, S. -C. Zhang, Quantum spin Hall effect and topological phase transition in HgTe quantum wells. *Science* **314**, 1757-1761 (2006).
  - [7] D. Hsieh, D. Qian, L. Wray, Y. Xia, Y. S. Hor, R. J. Cava, M. Z. Hasan, A topological Dirac insulator in a quantum spin Hall phase. *Nature* **452**, 970-974 (2008).
  - [8] E. I. Rashba, Properties of semiconductors with an extremum loop. I. Cyclotron and combinational resonance in a magnetic field perpendicular to the plane of the loop. *Soviet physics-Solid state* **2**, 1109-1122 (1960).
  - [9] G. Dresselhaus, Spin-orbit coupling effects in zinc blende structures. *Physical Review* **100**, 580 (1955).
  - [10] B. A. Bernevig, J. Orenstein, S. C. Zhang, Exact SU(2) symmetry and persistent spin helix in a spin-orbit coupled system. *Physical Review Letters* **97**, 236601 (2006).
  - [11] Y. J. Lin, K. Jiménez-García, I. B. Spielman, Spin-orbit-coupled Bose-Einstein condensates. *Nature* **471**, 83-86 (2011).
  - [12] J. R. Li, J. Lee, W. Huang, S. Burchesky, B. Shteynas, F. C. Top, A. O. Jamison, W. Ketterle, A stripe phase with supersolid properties in spin-orbit-coupled

- Bose–Einstein condensates. *Nature* **543**, 91-94 (2017).
- [13] Y. Li, L. P. Pitaevskii, S. Stringari, Quantum tricriticality and phase transitions in spin-orbit coupled Bose-Einstein condensates. *Physical Review Letters* **108**, 225301 (2012).
- [14] G. I. Martone, Y. Li, L. P. Pitaevskii, S. Stringari, Anisotropic dynamics of a spin-orbit-coupled Bose-Einstein condensate. *Physical Review A* **86**, 063621 (2012).
- [15] H. Zhai, Degenerate quantum gases with spin–orbit coupling: a review. *Reports on Progress in Physics* **78**, 026001 (2015).
- [16] C. Wang, C. Gao, C. M. Jian, H. Zhai, Spin-orbit coupled spinor Bose-Einstein condensates. *Physical Review Letters* **105**, 160403 (2010).
- [17] J. Radić, T. A. Sedrakyan, I. B. Spielman, V. Galitski, Vortices in spin-orbit-coupled Bose-Einstein condensates. *Physical Review A* **84**, 063604 (2011).
- [18] I. B. Spielman, Raman processes and effective gauge potentials. *Physical Review A* **79**, 063013 (2009).
- [19] J. Estève, C. Gross, A. Weller, S. Giovanazzi, M. K. Oberthaler, Squeezing and entanglement in a Bose–Einstein condensate. *Nature* **455**, 1216-1219 (2008).
- [20] G. B. Jo, Y. Shin, S. Will, T. A. Pasquini, M. Saba, W. Ketterle, D. E. Pritchard, M. Vengalattore, M. Prentiss, Long phase coherence time and number squeezing of two Bose-Einstein condensates on an atom chip. *Physical Review Letters* **98**, (2007).
- [21] K. Maussang, G. E. Marti, T. Schneider, P. Treutlein, Y. Li, A. Sinatra, R. Long, J. Estève, J. Reichel, Enhanced and reduced atom number fluctuations in a BEC splitter. *Physical Review Letters* **105**, 080403 (2010).
- [22] A. Itah, H. Veksler, O. Lahav, A. Blumkin, C. Moreno, C. Gordon, J. Steinhauer, Direct observation of a sub-Poissonian number distribution of atoms in an optical lattice. *Physical Review Letters* **104**, 113001 (2010).
- [23] J. C. Jaskula, M. Bonneau, G.B. Partridge, V. Krachmalnicoff, P. Deuar, K.V. Kheruntsyan, A. Aspect, D. Boiron, C. I. Westbrook, Sub-Poissonian number differences in four-wave mixing of matter waves. *Physical Review Letters* **105**, 190402 (2010).
- [24] N. Bozinovic, Y. Yue, Y. Ren, M. Tur, P. Kristensen, H. Huang, A. E. Willner, S. Ramachandran, Terabit-scale orbital angular momentum mode division multiplexing in fibers. *Science* **340**, 1545-1548 (2013).
- [25] Z. Zhang, H. Zhao, S. Wu, T. Wu, X. Qiao, Z. Gao, R. Agarwal, S. Longhi, N. M. Litchinitser, L. Ge, L. Feng, Spin–orbit microlaser emitting in a four-dimensional Hilbert space. *Nature* **612**, 246–251 (2022).
- [26] Z. Zhang, X. Qiao, B. Midya, K. Liu, J. Sun, T. Wu, W. Liu, R. Agarwal, J. M. Jornet, S. Longhi, N. M. Litchinitser, L. Feng, Tunable topological charge vortex microlaser. *Science* **368**, 760–763 (2020).
- [27] K. Rechcińska, M. Król, R. Mazur, P. Morawiak, R. Mirek, K. Łempicka, W. Bardyszewski, M. Matuszewski, P. Kula, W. Piecek, P.G. Lagoudakis, B. Piętka, J. Szczytko, Engineering spin-orbit synthetic Hamiltonians in liquid-crystal optical cavities. *Science* **366**, 727-730 (2019).
- [28] M. Król, K. Rechcińska, H. Sigurdsson, P. Oliwa, R. Mazur, P. Morawiak, W. Piecek, P. Kula, P. G. Lagoudakis, M. Matuszewski, W. Bardyszewski, B. Piętka, J. Szczytko, Realizing optical persistent spin helix and Stern-Gerlach deflection in an anisotropic liquid crystal microcavity. *Physical Review Letters* **127**, 190401 (2021).
- [29] J. Kasprzak, M. Richard, S. Kundermann, A. Baas, P. Jeambrun, J.M. Keeling, F.M. Marchetti, M.H. Szymańska, R. André, J.L. Staehli, V. Savona, P.B. Littlewood, B. Deveaud, S.L. Dang, Bose-Einstein condensation of exciton polaritons. *Nature* **443**, 409-414 (2006).
- [30] R. Balili, V. Hartwell, D. Snoke, L. Pfeiffer, K. West, Bose-Einstein condensation of microcavity polaritons in a trap. *Science* **316**, 1007-1010 (2007).
- [31] K.G. Lagoudakis, M. Wouters, M. Richard, A. Baas, I. Carusotto, R. André, L.S. Dang, B. Deveaud-Plédran, Quantized vortices in an exciton-polariton condensate. *Nature Physics* **4**, 706-710 (2008).
- [32] D. Sanvitto, F.M. Marchetti, M.H. Szymańska, G. Tosi, M. Baudisch, F.P. Laussy, D.N. Krizhanovskii, M.S. Skolnick, L. Marrucci, A. Lemaître, J. Bloch, C. Tejedor, L. Viña, Persistent currents and quantized vortices in a polariton superfluid. *Nature Physics* **6**, 527–533 (2010).
- [33] I. Ghusov, S. Harrison, S. Alyatkin, K. Sitnik, J. Töpfer, H. Sigurdsson, P. Lagoudakis, Quantum vortex formation in the “rotating bucket” experiment with polariton condensates. *Science Advances* **9**, eadd1299 (2023).
- [34] X. Ma, B. Berger, M. Assmann, R. Driben, T. Meier, C. Schneider, S. Hofling, S. Schumacher, Realization of all-optical vortex switching in exciton-polariton condensates. *Nature Communications* **11**, 897 (2020).
- [35] Y. del Valle-Inclan Redondo, C. Schneider, S. Klemmt, S. Höfling, S. Tarucha, M. D. Fraser, Optically Driven Rotation of Exciton-Polariton Condensates. *Nano Letters* **23**, 4564-4571 (2023).
- [36] Y. Li, X. Ma, X. Zhai, M. Gao, H. Dai, S. Schumacher, T. Gao, Manipulating polariton condensates by Rashba-Dresselhaus coupling at room temperature. *Nature Communications* **13**, 3785 (2022).
- [37] X. Zhai, X. Ma, Y. Gao, C. Xing, M. Gao, H. Dai, X. Wang, A. Pan, S. Schumacher, T. Gao, Electrically controlling vortices in a neutral exciton-polariton condensate at room temperature. *Physical Review Letters* **131**, 136901 (2023).
- [38] Y. Gao, X. Ma, X. Zhai, C. Xing, M. Gao, H. Dai, H. Wu, T. Liu, Y. Ren, X. Wang, A. Pan, W. Hu, S. Schumacher, and T. Gao, Single-shot spatial instability and electric control of polariton condensates at room temperature. *Physical Review B* **108**, 205303(2023).
- [39] M. S. Spencer, Y. Fu, A.P. Schlaus, D. Hwang, Y. Dai, M.D. Smith, D.R. Gamelin, X.-Y. Zhu, Spin-orbit coupled exciton-polariton condensates in lead halide perovskites. *Science Advances* **7**, eabj7667 (2021).
- [40] R. Su, J. Wang, J. Zhao, J. Xing, W. Zhao, C. Diederichs, T. C. H. Liew, Q. Xiong, Room temperature long-range coherent exciton polariton condensate flow in lead halide perovskites. *Science Advances* **4**, eaau0244 (2018).
- [41] K. Alexey, M. Guillaume, and G. Mikhail, Optical spin Hall effect. *Physical Review Letters* **95**, 136601 (2005).
- [42] C. Leyder, M. Romanelli, J. Ph. Karr, E. Giacobino, T. C. H. Liew, M. M. Glazov, A. V. Kavokin, G. Malpuech, and A. Bramati, Observation of the optical spin Hall effect. *Nature Physics* **3**, 628-631 (2007).
- [43] Terç H. Terças, H. Flayac, D. D. Solnyshkov, G. Malpuech, Non-Abelian gauge fields in photonic cavities and photonic superfluids. *Physical Review Letters* **112**, 066402 (2014).

- [44] X. Ma, Y. V. Kartasho, A. Kavokin, S. Schumacher, Chiral condensates in a polariton hexagonal ring. *Optics Letters* **45**, 5700-5703 (2020).
- [45] N. Carlon Zambon, P. St-Jean, M. Milićević, A. Lemaître, A. Harouri, L. Le Gratiet, O. Bleu, D.D. Solnyshkov, G. Malpuech, I. Sagnes, S. Ravets, A. Amo, J. Bloch, Optically controlling the emission chirality of microlasers. *Nature Photonics* **13**, 283-288 (2019).
- [46] V. G. Sala, D. D. Solnyshkov, I. Carusotto, T. Jacqmin, A. Lemaître, H. Terças, A. Nalitov, M. Abbarchi, E. Galopin, I. Sagnes, J. Bloch, G. Malpuech, and A. Amo, Spin-orbit coupling for photons and polaritons in microstructures. *Physical Review X* **5**, 011034 (2015).
- [47] M. Galbiati, L. Ferrier, D. D. Solnyshkov, D. Tanese, E. Wertz, A. Amo, M. Abbarchi, P. Senellart, I. Sagnes, A. Lemaître, E. Galopin, G. Malpuech, J. Bloch, Polariton condensation in photonic molecules. *Physical Review Letters* **108**, 126403 (2012).
- [48] L. Ferrier, E. Wertz, R. Johne, D. D. Solnyshkov, P. Senellart, I. Sagnes, A. Lemaître, G. Malpuech, J. Bloch, Interactions in confined polariton condensates. *Physical Review Letters* **106**, 126401 (2011).
- [49] L. Polimeno, G. Lerario, M. De Giorgi, L. De Marco, L. Dominici, F. Todisco, A. Coriolano, V. Ardizzone, M. Pugliese, C. T. Prontera, V. Maiorano, A. Moliterni, C. Giannini, V. Olieric, G. Gigli, D. Ballarini, Q. Xiong, A. Fieramosca, D. D. Solnyshkov, G. Malpuech, D. Sanvitto, Tuning of the Berry curvature in 2D perovskite polaritons. *Nature Nanotechnology* **16**, 1349 (2021).
- [50] K. Lempicka-Mirek, M. Król, H. Sigurdsson, A. Wincukiewicz, P. Morawiak, R. Mazur, M. Muszyński, W. Piecek, P. Kula, T. Stefaniuk, M. Kamińska, L. De Marco, P. G. Lagoudakis, D. Ballarini, D. Sanvitto, J. Szczytko, B. Piętka, Electrically tunable Berry curvature and strong light-matter coupling in liquid crystal microcavities with 2D perovskite. *Science Advances* **8**, eabq7533 (2022).